scientific reports

Check for updates

OPEN

RNA guanine content and G-quadruplex structure tune the phase behavior and material properties of biomolecular condensates

Alfredo Vidal Ceballos[1], Anna Geissmann[1,2], Denize C. Favaro[1], Priyasha Deshpande[1,3] & Shana Elbaum-Garfinkle[1,2,3,4]✉

RNA binding proteins (RBPs) are enriched in phase separated biomolecular assemblies across cell types. These RBPs often harbor arginine–glycine rich RGG motifs, which can drive phase separation, and can preferentially interact with RNA G-quadruplex (G4) structures, particularly in the neuron. Increasing evidence underscores the important role that RNA sequence and structure play in contributing to the form and function of protein condensates, however, less is known about the role of G4 RNAs and their interaction with RGG domains specifically. In this study we focused on the model protein, Fragile X mental retardation protein (FMRP), to investigate how G4-containing RNA sequences impact the phase behavior and material properties of condensates. FMRP is implicated in the development of Fragile X Syndrome, and is enriched in neuronal granules where it is thought to aid in mRNA trafficking and translational control. Here, we examined RNA sequences with increasing G content and G4 propensity in complex with the RGG-containing low complexity region (LCR) of FMRP. We found, that while increasing G content triggers aggregation of poly-arginine, all RNA sequences supported phase separation into liquid droplets with FMRP-LCR. Combining microrheology, and fluorescence recovery after photobleaching, we measured a moderate increase in viscosity and decrease in dynamics for increasing G-content, and detected no measurable increase in elasticity as a function of G4 structure. Additionally, we found that while methylation of FMRP decreased RNA binding affinity, this modification did not impact condensate material properties suggesting that RNA sequence/structure can play a greater role than binding affinity in determining the emergent properties of condensates. Together, this work lends much needed insight into the ways in which G-rich RNA sequences tune the assembly, dynamics and material properties of protein/RNA condensates and/or granules.

RNA binding proteins (RBPs) are enriched in numerous membraneless organelles, or biomolecular condensates, including neuronal granules, stress granules, and P-bodies[1,2] where they are implicated in processes such as mRNA transport, translational repression, and subcellular organization[3,4]. The arginine/glycine-rich RGG domain, found in over 1000 human RBPs, has been identified as a key driver of phase separation[5–9], and has been shown to be implicated in the recognition and preferential binding towards mRNAs containing G-quadruplex (G4) structure[10]. G4 mRNAs are non-canonical RNA structures made of at least two or more guanine quartets arranged via Hoogsteen base pairing and stabilized by monovalent cations (Fig. 1A)[11–13]. These secondary structures have relevant roles in neuronal function and disease[12] in addition to other biological processes such as DNA maintenance and replication[14]. Increasing evidence highlights the important role that RNA sequence and structure plays in contributing to the form and function of condensates, and in modulating their material properties[15–19]. RNA G4 structures, which have been shown to trigger aggregation and the formation of elastic networks in some systems[17,20], have the potential to significantly influence the material properties of condensates.

[1]Structural Biology Initiative, Advanced Science Research Center, CUNY, New York, NY, USA. [2]Ph.D. Program in Chemistry, Graduate Center of the City University of New York, New York, NY, USA. [3]Ph.D. Program in Biochemistry, Graduate Center of the City University of New York, New York, NY, USA. [4]Ph.D. Program in Biology, Graduate Center of the City University of New York, New York, NY, USA. ✉email: selbaumgarfinkle@gc.cuny.edu

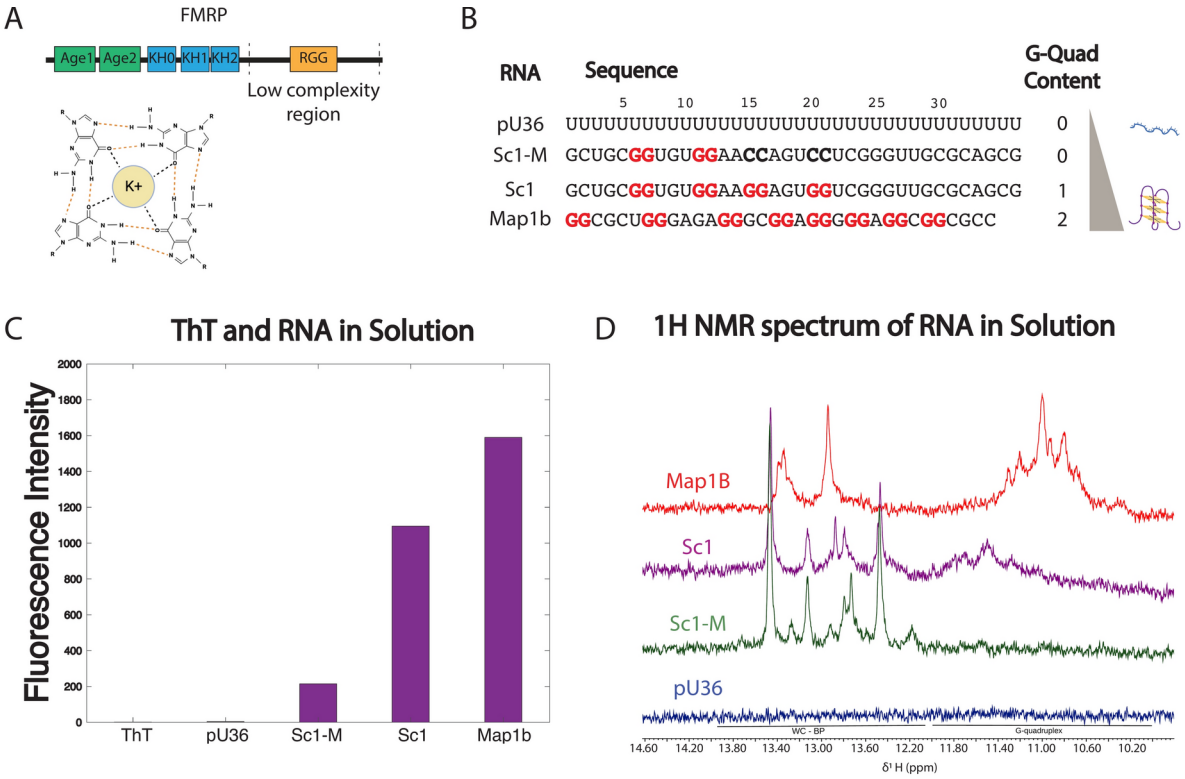

Fig. 1. RNA sequences and secondary structure characterization. (**A**) *Top* FMRP domain architecture which include the Agent like domains (Age) 1 and 2, K homology (KH) domains 0, 1, and 2, and the low complexity region (LCR) used in this study containing the RGG box domain (445–632) *Bottom* Four guanines forming a G-quartet via Hoogsteen base pairing stabilized by a potassium ion. (**B**) RNA identity and sequences used, poly-uridine 36 (pU36), Sc1, Sc1 mutant (Sc1-M) in which guanines 15–16 and 20–21 are replaced with cytosine, and microtubule associated protein 1 B (Map1B) and their corresponding QGRS scores. Highlighted in red are the guanines predicted to participate in the G4 structure. (C) Fluorescence intensity of ThT (5 μM) in the presence of different RNA identities (5 μM) measured at 487 nm. Buffer containing 25 mM $NaPO_4$, 20 mM KCl. (**D**) 1H solution NMR spectra of pU36 (Blue), Sc1-M (Green), Sc1 (Magenta), Map1B (Red) in buffer containing 50 μM $NaPO_4$, pH 7.4, 40 μM KCl at 25 °C.

The presence of G4s is also suggested to stabilize RBP disordered regions, promoting the structural character of the protein[21]. Although RBP containing RGG domains are documented to have a preferential binding to G4s in-vitro[11,22], whether G4s can influence the material properties of condensates formed by these RGG domain-containing proteins, remains to be determined.

In this study we focused on the model protein, Fragile X mental retardation protein (FMRP), to investigate how G4-containing RNA sequences impact the phase behavior and material properties of condensates. FMRP is associated with Fragile X Syndrome, a neurodevelopmental disorder that results in intellectual disabilities and behavioral issues such as hyperactivity and anxiety[23]. It is abundantly found in the neuron[24] and enriched in neuronal granules along with other RNA binding proteins, mRNA targets and polyribosomes[3]. The function of FMRP has been linked with translational repression and mRNA translocation in the neuron[25–27]. FMRP contains multiple RNA binding domains (Fig. 1A) and targets over ~ 1000 mRNA in the brain[3,27]. This broad range of RNA targets raises questions about the importance of FMRP-RNA binding specificity, as well as the effect of these RNAs on the material state of condensates. The low complexity region (LCR) of FMRP displays preferential binding affinity towards G4 mRNA[28,29], however, evidence for the relevance and specificity towards these secondary structures remains conflicting[21,27]. FMRP can undergo post-translational modifications, such as methylation and phosphorylation of its arginine residues[6] which has been shown to weaken its binding to RNA[30]. The RGG-containing LCR of FMRP is necessary and sufficient to induce the formation of condensates in solution[31,32], however, the emergent material properties of FMRP condensates and structured RNA remain unexplored. Here, we explore the modulation in material properties of FMRP-LCR condensates in the presence of increasingly complex RNA structure and guanine content. Additionally, we interrogate the role of arginine methylation, a common post translational modification, in condesate viscosity and dynamics.

Results

RNA sequence characterization

In order to measure the impact of G4 content on the phase behavior and material properties of condensates we examined 4 RNA sequences (Fig. 1B): Sc1 is a 36 nucleotide long synthetic RNA aptamer, that adopts G4 structure and is commonly used to study the interaction between the FMRP-LCR and RNA[11,33]. Mutating four specific guanines to cytosines in the Sc1 RNA sequence, referred to here-on as Sc1-M (Fig. 1B) is known to interfere with G4 structure formation by removing key guanines involved in the G-quartet stacking (Fig. 1B)[11]. We additionally selected the Microtubule associated protein 1B (Map1B), a key RNA in neuronal development, and native binding partner of the RGG domain of FMRP in the brain[34]. Map1B has a greater guanine content than Sc1, and based on online sequence predictor programs, has a higher quadruplex forming G-Rich Sequences (QGRS) score of 2 compared to 1 for Sc1 and 0 for Sc1-M (Fig. 1B)[35]. As a control for no structure as well as no G-content, we used Poly-Uridine 36 (pU36), an RNA homopolymer, that like Sc1-M has a QGRS score of 0.

To experimentally confirm the predicted G4 content of the RNA sequences, we first used Thioflavin T (ThT), a dye that undergoes a red shift when it intercalates with G4 secondary structure[36]. An increase in fluorescence signal was observed when G4-containing RNAs were incubated with ThT in solution (Fig. 1C). Consistent with the predicted G4 content, the fluorescence intensity increased proportionally, with the lowest value for pU36 (3.37), followed by Sc1-M (214.42), Sc1 (1095.12) and Map1B (1589.89). The greater signal noted for Map1B compared to Sc1 is consistent with the higher predicted QGRS score. However, to determine if the low level of ThT observed for Sc1-M was reflecting some residual G4 structure, we next used ^{1}H NMR spectroscopy. The presence of G4 structure is characterized by signature peaks in the region 10–12 ppm, which is detected for Sc1 and Map1B, but not for Sc1-M (Fig. 1D) indicating the absence of stable G4 structure for Sc1-M. Notably, the peaks for Map1B are sharper than the Sc1 peaks and have an overall signal/noise ratio increased by a factor of 2, which could be interpreted as more G4 structure. Interestingly, while no G4 structure was detected for Sc1-M via NMR at room temperature (Fig. 1D), G4 peaks were detected at 5 °C (Fig. S1), suggesting the possibility that Sc1-M forms more transient non-canonical secondary structures that cannot be detected due to increased hydrogen exchange among imino groups and water at room temperature, preventing them from being observed due to fast T2 relaxation.

High G-content promotes aggregation of homopolymers while forming spherical condensates with LCRs

While G4 RNAs are often associated with condensates comprised of RBPs harboring low complexity sequences, high guanine content in nucleic acids have also been shown to lead to the assembly of insoluble aggregates when combined with even less complex, positively charged polymers[17,18,20]. To reconcile the diverse phase behavior previously reported across different systems and conditions, we tested the phase behavior of our RNA sequences with the simple homopolymer poly-arginine in addition to FMRP, and other RBPs (Fig. 2, Fig. S2). Interestingly, we found that while arginine-rich FMRP-LCR can phase separate into spherical condensates with all the RNAs tested, the G4 containing RNAs Sc1 and Map1B lead to aggregate formation for poly-arginine under identical conditions that lead to spherical droplet formation with poly-uridine (Fig. 2 Top-Middle). This was also the case at much lower RNA concentrations (Fig. S3) indicating that the aggregation of the polymers is independent of RNA concentration. Interestingly, even the Sc1-M results in the formation of aggregates with poly-arginine, indicating that a stable G4 structure may not be required to induce aggregation. No aggregation was observed for any of our RNA sequences alone at the concentrations tested. These results demonstrate that the effect of G4 structure and/or G-content on phase behavior can depend strongly on the sequence complexity of its interaction partner. Notably, we observed spherical droplets with our RNAs for other proteins, including the RGG-containing protein LAF-1 (Fig. S2), indicating that the propensity for droplet formation with G4s is not specific to FMRP.

To assess whether G4 structure persisted within FMRP condensates, ThT was added to condensates formed with FMRP-LCR and each RNA. Like the measurements obtained in solution, an increase in fluorescence is observed within LCR-RNA condensates with increasing G4 RNA (Fig. 3). However, an almost fivefold increase in fluorescence intensity between FMRP-Sc1 and FMRP-Map1B condensates is observed (Fig. 3B), much greater than the 1.5-fold increase in ThT signal of free RNAs in solution (Fig. 1C). To see if this difference could be explained by a greater partitioning of Map1B into droplets, we measured the partition coefficient of labeled Map1B and Sc1 into droplets and found them to be equivalent (Fig. S4). We therefore speculate that there could be increased stabilization of the quadruplex in the case of Map1B, which is supported by an observed increase in ThT signal when FMRP is incubated with Map1B in solution (Fig. S5). We also cannot rule out the possibility that FMRP could be adopting alternative conformations in different condensate environments, that contributes to the overall ThT fluorescence.

G-content and not necessarily G4 structure decreases internal dynamics and increases viscosity of condensates

We next sought to investigate the internal environment of FMRP condensates when incubated with our array of distinct RNAs. We first used fluorescence recovery after photobleaching (FRAP) to measure the dynamics of fluorescently tagged FMRP-LCR inside the condensates (Fig. 4A,B). A recovery of ~ 99% fluorescence intensity was observed within 40 s for all RNA types. These results indicate that FMRP-RNA condensates remain highly dynamic even as the RNA secondary structure increases. This was initially surprising given that G4s have been shown to increase the formation of gel-like networks and aggregates when incubated with arginine-rich polymers[17,20] and (Fig. 2). Under closer inspection, however, the $\tau_{1/2}$, or the half time of recovery in the intensity graphs is observed to increase subtly as a function of RNA secondary structure (Fig. 4B), with FMRP-pU36 condensates having a $\tau_{1/2} = 4.9 \pm 0.4$ s and increasing to $\tau_{1/2} = 7.3 \pm 1.0$ s for FMRP-Map1B condensates.

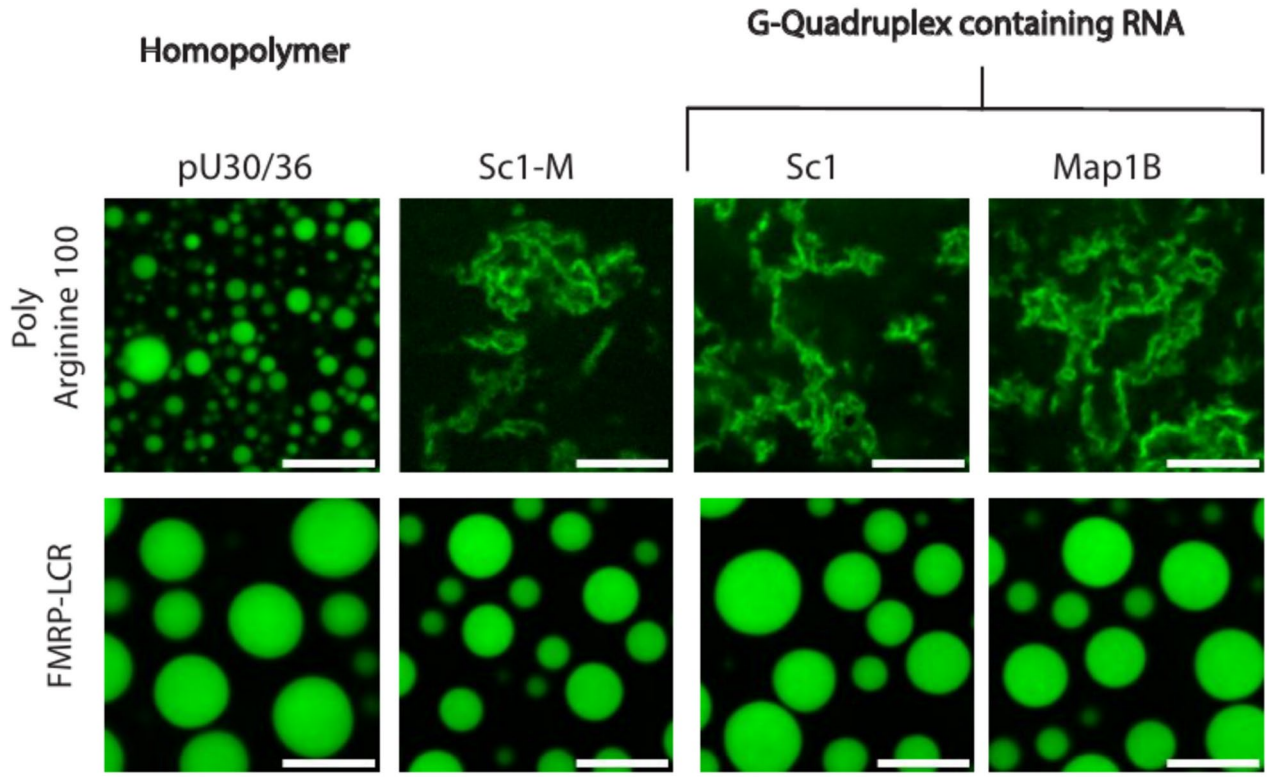

Fig. 2. (Top–Bottom) Condensate formation of Poly-Arginine 100, and the low complexity domain of (FMRP-LCR) in the presence of unstructured and G-quadruplex (G4) containing RNA labelled with Alexa488. Polymers where charge matched with their corresponding RNA, polymer concentration was 60 μM and RNA concentration was 200 μM, 167 μM, and 176 μM for pU30, Sc1, and Map1B respectively in buffer containing 10 mM Tris. FMRP condensates were induced at 150 μM protein and 10 μM RNA with all RNAs in buffer containing 25 mM $NaPO_4$, 20 mM KCl, 2 mM DTT. Scale bar 10 μm.

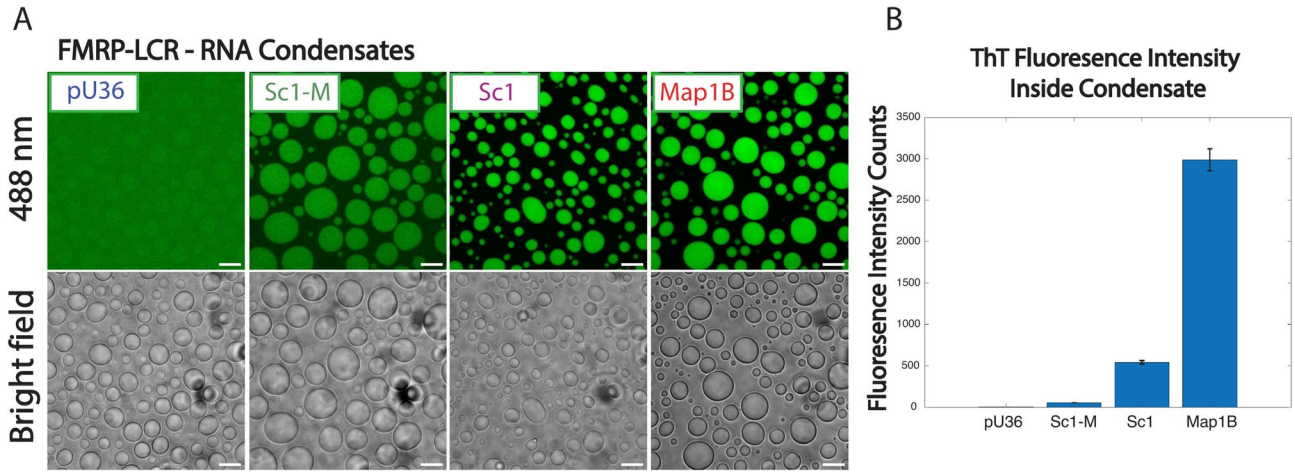

Fig. 3. G-quadruplex structure is preserved inside condensates. (**A**) Confocal microscopy image of FMRP-LCR condensates in the presence of different RNAs and ThT. (**B**) Normalized fluorescence intensity inside condensates. Error bar represents the standard deviation of intensity values of 3 distinct droplet samples. Protein concentration 150 μM, RNA 10 μM, ThT 5 μM in buffer containing 25 mM $NaPO_4$ pH 7.4, 20 mM KCl, 2 mM DTT.

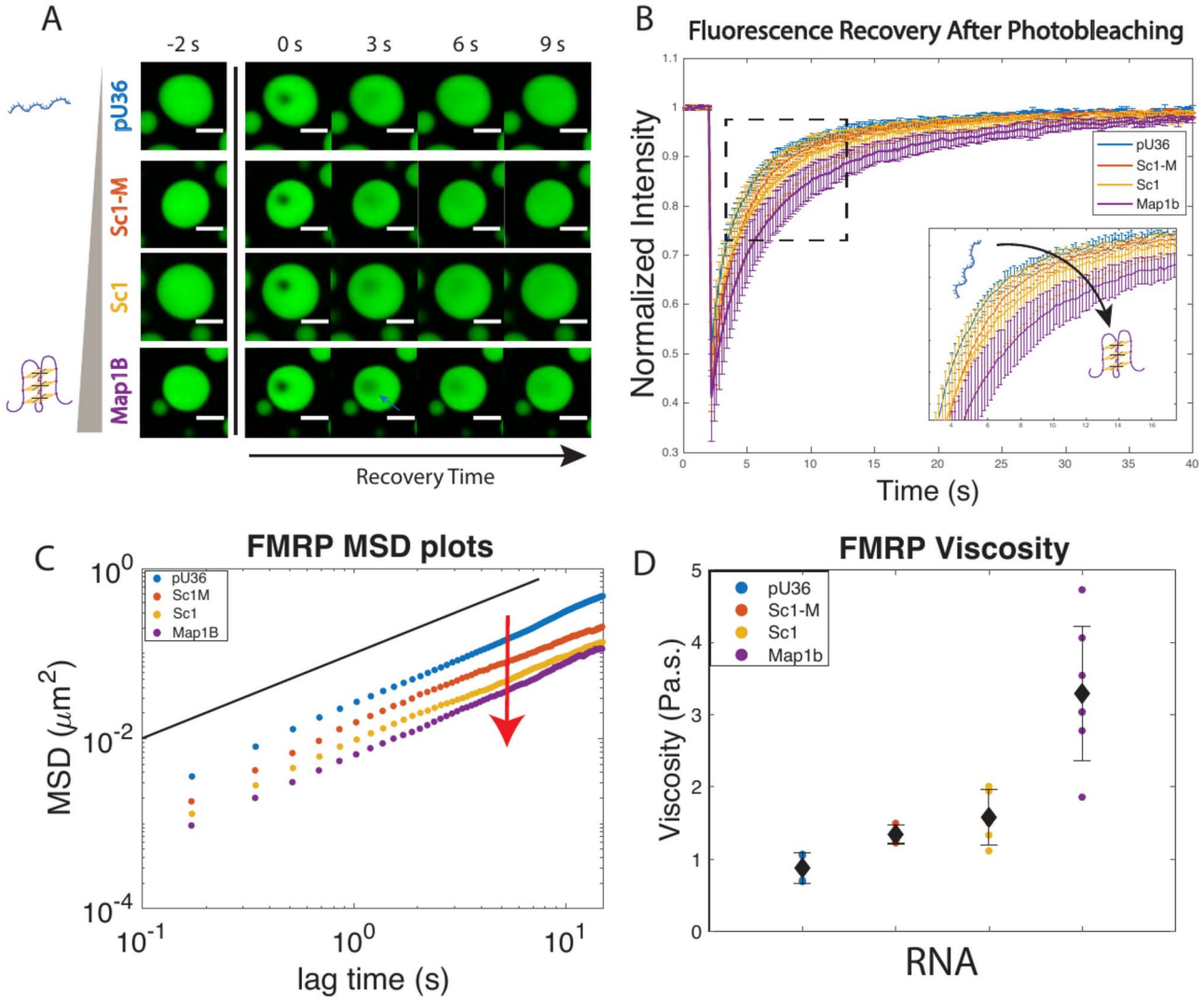

Fig. 4. G4 content decreases dynamics and increases viscosity inside FMRP condensates. (**A**) Confocal microscopy image sequences of fluorescently tagged FMRP-LCR incubated with pU36, Sc1-M, Sc1, and Map1B RNA respectively, recovering after photobleached as a function of time in seconds (scale bar 5 μm). (**B**) Normalized fluorescence recovery after photobleaching (FRAP) graphs in the presence of different RNA identities. Inset: Zoom in graph of mid-point fluorescence intensity recovery. Protein conditions: 150 μM FMRP-LCR, 10 μM RNA in buffer containing 25 mM NaPO4 pH 7.4, 20 mM KCl, 2 mM DTT. Protein labelled with Alexa488. (**C**) Average MSD of condensates incubated with increasing G4 RNA content (pU36 blue, Sc1M orange, Sc1 yellow, Map1B purple). Black line indicates slope of 1. (**D**) Viscosity values at increasing RNA G4 content (average viscosity in black diamond). Error bars reflect standard deviation. Protein conditions: 150 μM FMRP-LCR, 10 μM RNA in buffer containing 25 mM $NaPO_4$ pH 7.4, 20 mM KCl, 2 mM DTT. Microrheology was measured using 100 nm pegylated beads.

This indicates a small decrease in diffusion as the RNA G4 content increases, suggesting the G4 structure may influence the condensate material properties. We also observe a decrease in dynamics in LAF-1 condensates as the RNA secondary structure increases (Fig. S2). To extract information about the network properties of condensates as a function of RNA sequence we next employed particle tracking microrheology (Fig. 4C,D). In this technique fluorescent polystyrene beads that have been passivated using PEG are embedded in the FMRP condensates, and their diffusive motion is measured as a function of time. We found that the mean square displacement (MSD) had a linear dependance on lag time, resulting in a slope, or a diffusive exponent, of 1 for all RNAs (Fig. 4C) suggesting that condensates in the presence of all RNA identities remain viscous fluids within the time frame of the experiments. Using the Stokes Einstein equation, we measured the viscosity of the FMRP-RNA condensates. We found that the viscosity of FMRP condensates increases with G4 content, with 0.88 ± 0.2 Pa.s for pU36, increasing to 1.34 ± 0.1 for Sc1-M, 1.58 ± 0.4 for Sc1, and 3.29 ± 0.9 Pa.s. for Map1B RNA. Interestingly, there is a measurable increase in viscosity even for Sc1-M, consistent with the FRAP results discussed above, suggesting the possibility that G-content alone and not necessarily G4 structure influences the material properties of the droplet. In order to decouple these effects, we created a Sc1-shuffle sequence, that has

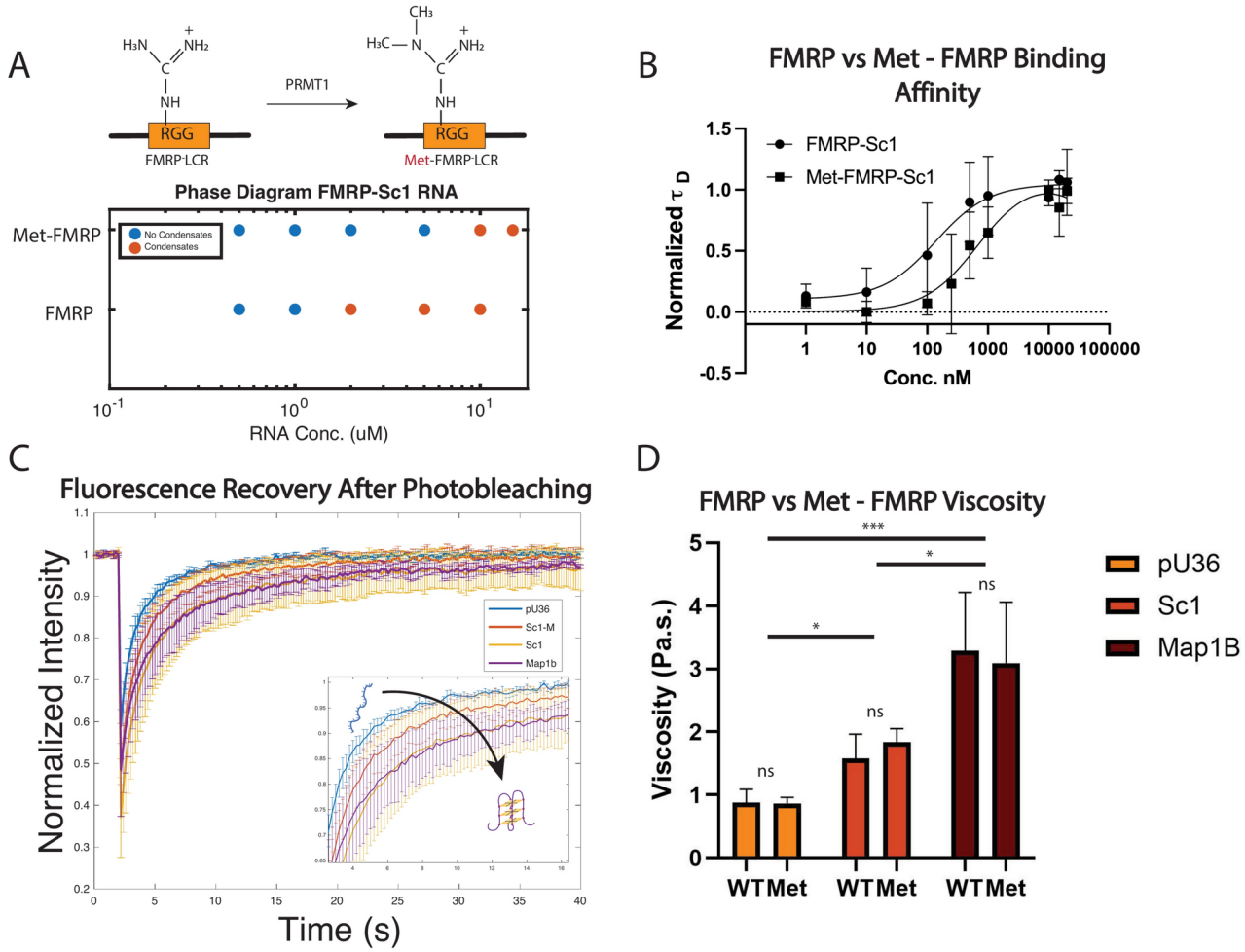

Fig. 5. Methylation of FMRP-LCR arginine's do not impact emergent material properties of FMRP-RNA condensates. (**A**) Top: schematic representation of RGG undergoing asymmetric di-methylation by PRMT1. Bottom: Phase diagram of wild type and methylated FMRP against RNA concentration. Protein concentration remained constant at 90 μM. (**B**) Binding curve representing normalized translational diffusion of labelled RNA against increasing FMRP concentration. (**C**) Normalized fluorescence recovery after photobleaching (FRAP) graphs of Met-FMRP condensates in the presence of different RNA identities of increasing G-quadruplex structures. Inset: Zoom in graph of mid-point fluorescence intensity recovery. (**D**) Comparison of measured viscosity values in Pa s. between WT and Methylated FMRP condensates. P-values were calculated using unpaired *t*-test comparing the mean, standard deviation, and number of repeats (N) between values. *ns* not significant.

the same number of G's as Sc1, but is predicted to have a QGRS score of 0. However, NMR spectra of this RNA depicted G4 formation (Fig. S6), so we did not proceed with this RNA. Based on this data we can thus conclude that increasing G-content, and not necessarily stable G4 structure decreases the dynamics and increases the viscosity of condensates in multiple systems.

Methylation of FMRP weakens RNA binding affinity but does not impact emergent material properties of FMRP-RNA condensates

Since it is known[11,33,37], and confirmed here (Fig. S7), that FMRP binds G4 sequences more tightly than unstructured RNA, it is difficult to conclude whether the condensate property changes measured are a result of increasing G content/G4 structure or increased binding affinity. In order to decouple the variables of binding affinity and G content, we next compared the phase behavior and properties of WT and methylated FMRP with a single RNA, Sc1. Methylated FMRP has been reported to bind Sc1 RNA with weakened affinity compared to WT—but the effect on condensate properties have yet to be determined.

Consistent with previous reports, we found that arginine methylation can modulate the phase separation propensity of FMRP in solution (Fig. 5A Bottom), by decreasing its phase propensity[6,38]. Upon addition of Sc1-RNA, methylated-FMRP was found to undergo phase separation, however the concentration of RNA required is higher (Fig. 5A). Using fluorescence correlation spectroscopy (FCS) we measured the binding affinity of methylated and non-methylated FMRP towards Sc1 RNA (Fig. 5B) to corroborate the decrease in binding

affinity between Met-FMRP and the RNA. We found that while Sc1–FMRP has a dissociation constant (K_D) of 136.5 nM, the K_D for Sc1-Met-FMRP increases to 574.3 nM. Sc1M–FMRP binding is similarly weakened with measured K_D of 538.9 nM (Fig. S7). We then measured the internal condensate dynamics using FRAP and microrheology. We find that the FRAP $\tau_{1/2}$ for pU36 is 3.09 s, increasing to 5.15 s for Sc1 and 5.42 s for Map1B, similarly to the results obtained for WT-FMRP. We also found that, like non-methylated FMRP condensates, we see a moderate increase in viscosity for Sc1 (1.84 ± 0.22 Pa·s) and Map1B (3.09 ± 0.97 Pa·s) compared to pU36 (0.87 ± 0.10 Pa·s). Remarkably, we did not observe any significant change in the viscosity of condensates when comparing FMRP and methylated FMRP for all RNAs tested (Fig. 5D). This suggests that RNA sequence and/or structure has a greater effect than binding affinity in dictating the material properties of the condensate. This data also demonstrates that changing the propensity to phase separate, illustrated by changes in the phase diagram, do not correlate with changes in material properties as measured here. In further support of this, we note that changes in the phase propensity of WT FMRP for distinct RNAs do not correlate with their G-content (Fig. S8), and their associated changes in material properties.

Discussion

This study aimed to decipher how RNA G4s influence phase behavior and material properties of condensates, and how these effects are tuned. We hypothesized that increasing RNA G4 structure would lead to a corresponding decrease in dynamics and increase in elasticity of condensates. Our results, however, support a more nuanced set of insights into the ways in which G4 structures can contribute to phase behavior and condensate properties.

First, while we do measure a difference in condensate viscosity and dynamics (Fig. 4) as a function of increasing G4 structure, we also detected incremental differences with Sc1-M which does not form stable G4 structure, suggesting that G-content may be the cause of the observed changes. While we designed our RNA sequences to increase in G4 structure, they also naturally increase in G-content, with Sc1-M, Sc1 and Map1B having 15 (42%), 19 (53%), and 22 (65%) G's respectively. To control for G-content, we designed a Sc1-Shuffled sequence predicted to have no G4 structure according to the QGRS score, but with the same number of Gs as Sc1. However, this sequence did in fact show G4 structure experimentally via NMR (Fig. S6), suggesting that it may be difficult to eliminate G4 structure when the RNA contains 50% G-content or above. Importantly, since we were able to detect non-canonical secondary structure in Sc1-M at lower temperatures (Fig. S1), we suspect that more dynamic and transient secondary structures could also be contributing to the changes in morphology (Fig. 2) and viscosity and dynamics (Fig. 4) of condensates. These insights might be particularly useful, given the debate about whether the formation of stable G4 structure is relevant for the recognition between the RGG domains of FMRP and its RNA targets[39]. Evidence for the specificity of FMRP towards a particular secondary RNA structure is conflicting, with studies confirming that G4 present in the 3′ untranslated regions[40], as well as the coding regions of mRNA aid in binding and transport[28]; Conversely, Darnell and colleagues find no specific RNA sequence or structure preferred by the protein[27].

Second, given the previous studies on G4 structures promoting aggregation in some systems, and seen in this work for poly-arginine (Fig. 2 Top)[17,20] we hypothesized that increasing G4 structure would increase the elasticity of the FMRP condensates and even lead to morphological changes and/or heterogeneity in the system. Surprisingly, there is no significant deviation from a diffusive exponent of 1 as observed in our microrheology data, which depicts a fluid system at the time scale of our measurment. Additionally, the system remains highly dynamic by FRAP for all RNAs tested. However, we do measure a moderate increase in viscosity, and decrease in dynamics as a function of increasing G-content (Fig. 4). It has been suggested that FMRP might play a protective role against aggregation in TDP-43 containing granules[41]. Moreover, mutations to the *FMR1* gene that results in a toxic version of FMRP with a prion-like domain results in the toxic aggregation of the protein when interacting with G4s in the cell[42] suggesting that a healthy FMRP may play a role in preventing aggregation when interacting with G4 RNAs. It is tempting to speculate that perhaps FMRP plays a role in maintaining fluid properties in neuronal granules that sequester large amounts of aggregation-prone G-rich sequences. Additionally, it will be illuminating to better understand the nature of the distinct assembly behaviors observed for simple polymers versus more complex sequences like RGG domains (Fig. 2).

Third, we demonstrated that altering binding affinity does not necessarily influence material properties of condensates. Condensate formation relies on weak and dynamic interactions which can often be tuned by the relative interactions strengths[43]. Here, we showed that while methylation of FMRP decreases RNA binding, these changes have no significant effect on the material properties of condensates. We suspect that, although methylation may have an effect in phase separation propensity and binding affinity towards its mRNA target, once phase separation occurs, it is the RNA sequence and/or structure that then dictates the material properties of FMRP-RNA condensates. Additionally, we observe no trend in the phase propensity of WT FMRP as a function of RNA G content (Fig. S8), additionally suggesting that changes in propensity to phase separate are not necessarily linked to changes in material properties.

This work, which demonstrates the impact of RNA G-content and G4 structures on condensate dynamics, supports growing attention to the role of RNA in modulating the form and function of condensates, and is particularly relevant for understanding granule dynamics in neurons, where G4 structures are implicated in transport, translation and subcellular localization[12,14,44].

Materials and methods

Wild type and methylated FMRP-low complexity region (LCR) purification protocol

The human FMRP low complexity region (445–632 GASSRPPPNRTDKEKSYVTDDGQGMGRGSRPYRN-RGHGRRGPGYTSGTNSEASNASETESDHRDELSDWSLAPTEEERESFLRRGDGRRRGGGGRGQGGRGRG-GGFKGNDDHSRTDNRPRNPREAKGRTTDGSLQIRVDCNNERSVHTKTLQNTSSEGSRLRTGKDRNQK-

KEKPDSVDGQQPLVNGVP) was purified as previously described[31,38]. The plasmid LCR plasmid (Champion™ pET-SUMO) with the FMRP-LCR insert was resuspended in deionized water before transforming in *Escherichia coli* (*E. coli*) BL21 cells for expression and DH5α cells for storage. His-SUMO-FMRP was transformed into BL21 cells and grown in LB broth at 37 °C. The cells were induced with a final concentration of 0.5 mM Isopropil β-d-thiogalactopyranoside (IPTG) per liter of cells at an OD 600 value between 0.6 and 0.8 after which they were left in incubator at 24 °C overnight (20 h). Cells were harvested after growth at 4000 rpms at 4 °C. Cells were stored at − 80 °C or used immediately after this step. Cells were lysed in buffer containing 50 mM Tris (pH 8) 500 mM NaCl, 6 M Gdn-HCl and 2 mM β-mercaptoethanol (βME) and sonicated 4.5 min (2 s on, 1 s off) at 30% power. Lysed cell pellets were centrifuged at 18,000 RPM for 45 min to 1 h and supernatant was collected and filtered through 1 um filter. Supernatant was run through nickel gravity column (1 mL of slurry per 1 L of cell growth) equilibrated in 10 column volumes of lysis buffer. Column was washed with 5 column volumes of lysis buffer and buffer exchanged in buffer containing 50 mM Tris (pH 8), 500 mM NaCl, 2 mM (βME). Protein was eluted with buffer containing 50 mM Tris (pH 8), 500 mM NaCl, 2 mM βME and 300 mM imidazole.

Fractions that contain protein (confirmed either by absorbance at 280 or running a gel) are collected and placed into dialysis bag along with ULP enzyme (1:500) to remove the His-SUMO tag (ULP enzyme purified in lab, see next section for protocol), against buffer containing 50 mM tris (pH 8), 150 mM NaCl, 2 mM βME and left overnight at room temperature to remove imidazole. Next day, some lysis buffer was added (until samples is ~ 2 M Gdn-HCl) to dissolve any visible aggregates. Sample was loaded onto nickel column and flow through was collected to obtain cleaved FMRP protein. The His-SUMO tail was eluted with elution buffer and ran on an SDS-PAGE gel to obtain fractions with pure protein. The fractions with protein were combined and concentrated to ~ 2.5 mL and ran through a Superdex75 size exclusion column equilibrated with 50 mM Tris (pH 8), 150 mM NaCl, 2–3 M Gdn HCl, 2 mM βME. Pure protein was collected and concentrated to a desired concentration for experiments and diluted to a final concentration of 10% glycerol before being flash frozen with liquid nitrogen and stored at − 80 °C until further used.

FMRP methylation

The FMRP-LCR protein was methylated via co-expression of protein arginine *N*-methyltranferase 1 (PRMT1) plasmid[45] along with FMRP-LCR plasmid. The methylation of the protein was corroborated using mass spectrometry (Fig. S9) which gave a difference of ~ 160 Da between wild type and methylated protein, an addition of ~ 10 methyl groups, suggesting complete asymmetric methylation of ~ 5 arginine, or partial methylation of multiple arginine residues.

Protein labelling

FMRP-LCR was labelled using Alexa Fluor 488 C5—Maleimide (ThermoFisher Scientific) per the manufacturer instructions. Briefly, 75 µL containing 54 µM protein was diluted for a final × 7 excess unreacted dye in buffer containing 25 mM $NaPO_4$ and 2 mM tris(2-carboxyethyl)phosphine (TCEP). After 2 h of incubation, the reaction was quenched using solution containing excess DTT. The labelled peptide was washed using a 10 kD Amicon filter in a tabletop centrifuge and buffer exchanged with fresh buffer until the absorbance (488 nm) in the flow through reached 0. Labelling was confirmed by measuring the absorption of the product at 280 and 493 nm to determine the concentration of labelled protein.

pULP (SUMO Protease) purification

The plasmid was transformed into BL21 cell for expression and DH5α cells for storage. BL21 cells were streaked in Kanamycin resistant LB plates overnight. Single colony was added to 4 mL of LB broth with 20 µL Kanamycin (20 mg/mL) added and left for incubation for 5 h. 1 mL was transferred to 100 mL LB (with 100 µL of Kanamycin) and incubated at 37 °C overnight. 1 L LB (with 1 mL Kanamycin) broth was inoculated with 100 mL LB and induced with 1 mL IPTG (1 M) at an OD600 of 0.6 and left to grow at 37 °C until no change in OD600 is observed (4–5 h with an OD ~ 1–1.2). The bacteria were harvested and either proceeded with purification or stored at − 80 °C for later use. The bacterial pellets were resuspended with ~ 25 mL Lysis buffer (350 mM NaCl, 20 mM Imidazole, 20 mM Tris pH 8, 1.5 mM βME, 2 mM DTT). Lysate was sonicated for 6 min (5 s on/5 s off) at 40% amplitude. Cell lysate was centrifuged at 24,000 rpm for 1 h at 4 °C and clear lysate was collected. About ~ 1.2 mL of Nickle slurry (3.5 mL Nickel gravity column) was used per every liter of bacterial growth. Nickel beads were equilibrated with 5 × lysis buffer (50 mL), after which the clear lysate was ran through the column and flow through was collected. Column was washed with 45 mL of wash buffer (350 mM NaCl, 20 mM Imidazole, 20 mM Tris pH 8.0, 1.5 mM βME, 2 mM DTT). ULP was eluted with elution buffer (350 mM NaCl, 250 mM Imidazole, 20 mM Tris pH 8.0, 1.5 mM βME, 2 mM DTT). Elution fractions were checked with SDS PAGE gel and fractions with protein were pooled together and dialyze against PBS buffer (50 mM NaPi, 300 mM NaCl, pH 8.0, 1 mM DTT) at 4 °C. Molecular weight: 31,000 Da, extinction coefficient: 30,035 M^{-1} cm^{-1}.

Condensate preparation

FMRP-LCR protein was buffer exchanged into working buffer (25 mM $NaPO_4$, 20 mM KCl, 2 mM DTT) and concentrated using a 10-kDa cutoff Amicon ultra-centrifugal filter unit until a desired concentration (~ 210 µM) was achieved. The stock was used to dilute the protein to working concentration and the desired amount of RNA in a microscope glass slide previously washed with 70% ethanol and incubated with 1% Pluronics F-127 for 45 min. The samples were let incubate between 45 min and 2 h depending on the experiment. For microrehology measurements droplets not let to incubate longer than ~ 2.5 h for all experiments to prevent possible artificial maturation. Condensates are induced when RNA was added into the slide. All buffers containing NaPO4 were created as follows: 100 mM NaPO4 buffer stock was created by using a mixture of Na2HPO4 (77.4 mM final

concentration) and NaH2PO4 (22.6 mM final concentration) pH was checked or adjusted accordingly for a final pH of 7.4. This stock was further diluted to the desired concentration for experimental and imaging assays.

Fluorescence spectroscopy measurement

The fluorescence spectra were acquired in a SpectraMax i3 using a 96-well plate. The final concentration of Thioflavin T (ThT) and RNA was 5 µM and 5 µM respectively in buffer containing 25 mM $NaPO_4$ pH 7.4 and 20 mM KCl. The measurements were performed at 25 °C at an excitation of 440 nm and emission of 487 nm following a previously established protocol[36].

Solution-state NMR spectroscopy

NMR experiments were performed on a Bruker Avance III HD spectrometer operating at a ^1H frequency of 700.20 MHz and equipped with a 5-mm QCl CryoProbe probe with z-gradient and temperature control. RNA samples at a final concentration of 150 µM were prepared by adding 10% (v/v) D_2O to the samples buffered with 50 mM phosphate and 40 mM KCl at 7.4 pH. The experiments (Fig. 1D) were acquired at 25 °C and 5 °C (Fig. S7) using excitation-sculpting for water suppression using the same number of points (TD) of 16,384 points, receiver gain of 203, recycling delay of 1 s, and number of scans of 8192. All the experiments were acquired using 1.7 mm tubes (50 µL). NMRFx Analyst was used for processing and analysis.

FRAP

Fluoresence recovery after photobleaching (FRAP) experiments were performed for Alexa-488 labeled FMRP-LCR. Briefly, a small amount (~ 1%) of labeled protein is mixed with unlabeled protein before coacervation is induced. The final concentration of protein was 150 µM and phase separation was induced using 10 µM RNA. A 0.5 mm sized area is photobleached within the condensate, and the recovery of fluorescence is tracked as a function of time. FRAP images were acquired using a Marianas Spinning Disk confocal microscope with a × 63/1.4 NA (Intelligent Imaging Innovations, Denver, CO). Alexa 488 was excited using the 488-nm line from a solid-state laser (LaserStack). Correction for photobleaching, normalization, and fitting the recovery of fluorescence was plotted as a function of time and fitted using exponential function of the form

$$I_{fit} = I_0 - a \cdot e^{(-\beta \cdot t)} - g^{(-\delta \cdot t)}.$$

ImageJ was used to process the images, and the recovery of fluorescence was normalized using MATLAB to obtain the mobile fraction (I_0) and half-time of recovery [ln(2)/β]. The temperature was maintained using a microfluidics temperature stage (CherryTemp, CherryBiotech) at 23 °C.

Microrheology

Microrheology experiments were carried it out using a Marianas Spinning Disk confocal microscope with a × 63/1.4 NA Plan-Achromat oil objective. The temperature was maintained using a microfluidics temperature stage (CherryTemp, CherryBiotech) at 23 °C. 100 nm carboxylate beads with Polyethylene-glycol (PEG) passivated surface were used for particle tracking. The particle tracking code was to locate and trace trajectories in two dimensions (X and Y) was adapted from MATLAB Multiple Particle Tracking Code from the MATLAB particle tracking code repository (https://site.physics.georgetown.edu/matlab)[5,46]. The Mean-square displacement of the beads was calcilated from time and ensample averages for all trajectories:

$$MSD\,(\tau) = < (x\,(\tau + t) - x\,(t)\,)^2 > + < y(\tau + t)^2 > .$$

The dependence of the MSD on lag time (τ) follows a power law; the exponent α was determined as the slope of a log–log plot and diffusion coefficient as the y intercept:

$$MSD\,(\tau) = 2dD\tau^{\alpha},$$

where d is the number of dimensions, D is the diffusion coefficient, and α is the exponent. Viscosity can be determined from the Stokes–Einstein relation, assuming a system at equilibrium and a freely diffusing Brownian particle within a solution of viscosity η. The final viscosity is the average of three values collected from individual measurements performed on 3 different days at 23 °C ± 2 °C.

Mass spectrometry

MALDI-TOF mass spectrometry measurements were performed using a Bruker Autoflex Speed TOF/TOF instrument and the matrix was prepared by dissolving 10 mg of sinapic acid in 1 mL of buffer containing 70% acetonitrile, 27% water, and 3% acetic acid. 10 µM proteins was combined with the matrix in a 1:1 ratio and 1 µL was left to dry before measurement took place.

Fluorescence correlation spectroscopy experiments

The binding affinity between FMRP-LCR/Met-FMRP-LCR and the different RNAs was determined using fluorescence correlation spectroscopy (FCS) to measure the translational diffusion of fluorescently labelled RNA (Alexa-488) as an increasing amount of unlabeled protein was added. The FCS binding measurements were collected using an inverted Leica TCS SP8 STED 3X with a 63× water immersion objective. The fluorophore was excited at 488 nm and the detection window was between 498 and 510 nm using a HyD detector. The data was analyzed using SymPhoTime (PicoQuant, Germany) software, with each measurement being an average of 300 s

traces to obtain the correlation curves $G(\tau)$. The average correlation curves were fitted to a single-component triplet model using the equation:

$$G(\tau) = \left[1 + T\left[\exp\left(-\frac{t}{\tau_{Trip}}\right) - 1\right]\right] \times \frac{1}{\left[\mathrm{N}\left(1 + \frac{\tau}{\tau_D}\right)\left(1 + \frac{\tau}{\kappa^2\tau_D}\right)^{0.5}\right]},$$

where $G(\tau)$ is the autocorrelation function as a function of time τ. N is the average number of molecules in the focal volume. τ_D is the average diffusion time of fluorescence molecules through the focal volume. $\kappa = \frac{z_0}{\omega_0}$ represents the ratio of the axial z_0 and radial dimensions ω_0 of the Gaussian excitation volume. T is the dark (triplet) fraction of molecules, and τ_{Trip} is the lifetime of the dark (triplet) state. The focal volume was determined using Atto-488-carboxylic acid ($D = 4.0 \times 10^{-6}$ cm^2 s^{-1}) at 25 °C. The τ_D of the fluorescently labelled RNA at increasing protein concentration was measured and fitted using Prism 9 with a one-site total binding model:

$$Y = \frac{B_{max} \times X}{Kd + X} + NS \times X + B,$$

where B_{max} is the maximum specific binding, Kd in the equilibrium dissociation constant in nM, and NS is the slope of the non-specific binding.

Received: 4 September 2024; Accepted: 28 January 2025
Published online: 18 March 2025

References

1. Prashad, S. & Gopal, P. P. RNA-binding proteins in neurological development and disease. *RNA Biol.* **18**, 972–987 (2021).
2. Vanderweyde, T., Youmans, K., Liu-Yesucevitz, L. & Wolozin, B. Role of stress granules and RNA-binding proteins in neurodegeneration: A mini-review. *Gerontology* **59**, 524–533 (2013).
3. El Fatimy, R. et al. Tracking the fragile X mental retardation protein in a highly ordered neuronal ribonucleoparticles population: A link between stalled polyribosomes and RNA granules. *PLoS Genet.* **12**, e1006192 (2016).
4. Bauer, K. E., de Queiroz, B. R., Kiebler, M. A. & Besse, F. RNA granules in neuronal plasticity and disease. *Trends Neurosci.* **46**, 525–538 (2023).
5. Elbaum-Garfinkle, S. et al. The disordered P granule protein LAF-1 drives phase separation into droplets with tunable viscosity and dynamics. *Proc. Natl. Acad. Sci. U.S.A.* **112**, 7189–7194 (2015).
6. Tsang, B. et al. Phosphoregulated FMRP phase separation models activity-dependent translation through bidirectional control of mRNA granule formation. *Proc. Natl. Acad. Sci. U.S.A.* **116**, 4218–4227 (2019).
7. Nott, T. J. et al. Phase transition of a disordered nuage protein generates environmentally responsive membraneless organelles. *Mol. Cell* **57**, 936–947 (2015).
8. Saha, S. et al. Polar positioning of phase-separated liquid compartments in cells regulated by an mRNA competition mechanism. *Cell* **166**, 1572–1584 (2016).
9. Spaulding, E. L., Feidler, A. M., Cook, L. A. & Updike, D. L. RG/RGG repeats in the *C. elegans* homologs of Nucleolin and GAR1 contribute to sub-nucleolar phase separation. *Nat. Commun.* **13**, 6585 (2022).
10. Brazda, V. et al. The amino acid composition of quadruplex binding proteins reveals a shared motif and predicts new potential quadruplex interactors. *Molecules* **23**, 1 (2018).
11. Darnell, J. C. et al. Fragile X mental retardation protein targets G quartet mRNAs important for neuronal function. *Cell* **107**, 489–499 (2001).
12. Asamitsu, S. et al. Perspectives for applying G-quadruplex structures in neurobiology and neuropharmacology. *Int. J. Mol. Sci.* **20**, 1 (2019).
13. Kharel, P., Becker, G., Tsvetkov, V. & Ivanov, P. Properties and biological impact of RNA G-quadruplexes: From order to turmoil and back. *Nucleic Acids Res.* **48**, 12534–12555 (2020).
14. Xu, J., Huang, H. & Zhou, X. G-quadruplexes in neurobiology and virology: Functional roles and potential therapeutic approaches. *JACS Au* **1**, 2146–2161 (2021).
15. Langdon, E. M. et al. mRNA structure determines specificity of a polyQ-driven phase separation. *Science* **360**, 922–927 (2018).
16. Zhang, H. et al. RNA controls PolyQ protein phase transitions. *Mol. Cell* **60**, 220–230 (2015).
17. Boeynaems, S. et al. Spontaneous driving forces give rise to protein-RNA condensates with coexisting phases and complex material properties. *Proc. Natl. Acad. Sci. U.S.A.* **116**, 7889–7898 (2019).
18. Roden, C. & Gladfelter, A. S. RNA contributions to the form and function of biomolecular condensates. *Nat. Rev. Mol. Cell Biol.* **22**, 183–195 (2021).
19. Putnam, A., Cassani, M., Smith, J. & Seydoux, G. A gel phase promotes condensation of liquid P granules in *Caenorhabditis elegans* embryos. *Nat. Struct. Mol. Biol.* **26**, 220–226 (2019).
20. Guo, W. et al. Tuning material states and functionalities of G-quadruplex-modulated RNA-peptide condensates. *J. Am. Chem. Soc.* **145**, 2375–2385 (2023).
21. Ozdilek, B. A. et al. Intrinsically disordered RGG/RG domains mediate degenerate specificity in RNA binding. *Nucleic Acids Res.* **45**, 7984–7996 (2017).
22. Ramos, A., Hollingworth, D. & Pastore, A. G-quartet-dependent recognition between the FMRP RGG box and RNA. *RNA* **9**, 1198–1207 (2003).
23. Richter, J. D. & Zhao, X. The molecular biology of FMRP: New insights into fragile X syndrome. *Nat. Rev. Neurosci.* **22**, 209–222 (2021).
24. Siomi, H., Siomi, M. C., Nussbaum, R. L. & Dreyfuss, G. The protein product of the fragile X gene, FMR1, has characteristics of an RNA-binding protein. *Cell* **74**, 291–298 (1993).
25. Shiina, N. & Tokunaga, M. RNA granule protein 140 (RNG140), a paralog of RNG105 localized to distinct RNA granules in neuronal dendrites in the adult vertebrate brain. *J. Biol. Chem.* **285**, 24260–24269 (2010).
26. Antar, L. N., Afroz, R., Dictenberg, J. B., Carroll, R. C. & Bassell, G. J. Metabotropic glutamate receptor activation regulates fragile x mental retardation protein and FMR1 mRNA localization differentially in dendrites and at synapses. *J. Neurosci.* **24**, 2648–2655 (2004).

27. Darnell, J. C. et al. FMRP stalls ribosomal translocation on mRNAs linked to synaptic function and autism. *Cell* **146**, 247–261 (2011).
28. Goering, R. et al. FMRP promotes RNA localization to neuronal projections through interactions between its RGG domain and G-quadruplex RNA sequences. *Elife* **9**, 1 (2020).
29. Athar, Y. M. & Joseph, S. RNA-binding specificity of the human fragile X mental retardation protein. *J. Mol. Biol.* **432**, 3851–3868 (2020).
30. Dolzhanskaya, N., Merz, G., Aletta, J. M. & Denman, R. B. Methylation regulates the intracellular protein–protein and protein–RNA interactions of FMRP. *J. Cell Sci.* **119**, 1933–1946 (2006).
31. Vernon, R. M. et al. Pi-Pi contacts are an overlooked protein feature relevant to phase separation. *Elife* **7**, 1 (2018).
32. Tsuruta, M. et al. Controlling liquid–liquid phase separation of G-quadruplex-forming RNAs in a sequence-specific manner. *Chem. Commun. (Camb.)* **58**, 12931–12934 (2022).
33. Phan, A. T. et al. Structure-function studies of FMRP RGG peptide recognition of an RNA duplex-quadruplex junction. *Nat. Struct. Mol. Biol.* **18**, 796–804 (2011).
34. Menon, L., Mader, S. A. & Mihailescu, M. R. Fragile X mental retardation protein interactions with the microtubule associated protein 1B RNA. *RNA* **14**, 1644–1655 (2008).
35. Kikin, O., D'Antonio, L., Bagga, P. S. & Mapper, Q. G. R. S. A web-based server for predicting G-quadruplexes in nucleotide sequences. *Nucleic Acids Res.* **34**, W676–W682 (2006).
36. Xu, S. et al. Thioflavin T as an efficient fluorescence sensor for selective recognition of RNA G-quadruplexes. *Sci. Rep.* **6**, 24793 (2016).
37. Vasilyev, N. et al. Crystal structure reveals specific recognition of a G-quadruplex RNA by a beta-turn in the RGG motif of FMRP. *Proc. Natl. Acad. Sci. U.S.A.* **112**, E5391–E5400 (2015).
38. Kim, T. H. et al. Phospho-dependent phase separation of FMRP and CAPRIN1 recapitulates regulation of translation and deadenylation. *Science* **365**, 825–829 (2019).
39. Li, M. et al. Identification of FMR1-regulated molecular networks in human neurodevelopment. *Genome Res.* **30**, 361–374 (2020).
40. Zhang, Y., Gaetano, C. M., Williams, K. R., Bassell, G. J. & Mihailescu, M. R. FMRP interacts with G-quadruplex structures in the 3'-UTR of its dendritic target Shank1 mRNA. *RNA Biol.* **11**, 1364–1374 (2014).
41. Coyne, A. N. et al. Fragile X protein mitigates TDP-43 toxicity by remodeling RNA granules and restoring translation. *Hum. Mol. Genet.* **24**, 6886–6898 (2015).
42. Asamitsu, S. et al. CGG repeat RNA G-quadruplexes interact with FMRpolyG to cause neuronal dysfunction in fragile X-related tremor/ataxia syndrome. *Sci. Adv.* **7**, 1 (2021).
43. Banani, S. F., Lee, H. O., Hyman, A. A. & Rosen, M. K. Biomolecular condensates: Organizers of cellular biochemistry. *Nat. Rev. Mol. Cell Biol.* **18**, 285–298 (2017).
44. Simone, R., Fratta, P., Neidle, S., Parkinson, G. N. & Isaacs, A. M. G-quadruplexes: Emerging roles in neurodegenerative diseases and the non-coding transcriptome. *FEBS Lett.* **589**, 1653–1668 (2015).
45. Stetler, A. et al. Identification and characterization of the methyl arginines in the fragile X mental retardation protein Fmrp. *Hum. Mol. Genet.* **15**, 87–96 (2006).
46. Fisher, R. S. & Elbaum-Garfinkle, S. Tunable multiphase dynamics of arginine and lysine liquid condensates. *Nat. Commun.* **11**, 4628 (2020).

Author contributions

AVC and SEG designed experiments and wrote the manuscript; AG and DF performed and analyzed NMR experiments; PD and AVC created the methylated FMRP.

Declarations

Competing interests

There are no competing interests.

Additional information

Supplementary Information The online version contains supplementary material available at https://doi.org/10.1038/s41598-025-88499-y.

Correspondence and requests for materials should be addressed to S.E.-G.